IEEE Access
Multidisciplinary | Rapid Review | Open Access Journal

Received January 19, 2021, accepted January 21, 2021, date of publication January 26, 2021, date of current version February 16, 2021.

*Digital Object Identifier 10.1109/ACCESS.2021.3054653*

# Dynamical Analysis and Sampled-Data Stabilization of Memristor-Based Chua's Circuits

**NALLAPPAN GUNASEKARAN[1,2], SABARATHINAM SRINIVASAN[3], GUISHENG ZHAI[1], (Senior Member, IEEE), AND QIANG YU[4], (Member, IEEE)**

[1]Department of Mathematical Sciences, Shibaura Institute of Technology, Saitama 337-8570, Japan
[2]Computational Intelligence Laboratory, Department of Advanced Science and Technology, Toyota Technological Institute, Nagoya 468-8511, Japan
[3]Centre for Nonlinear Dynamics, School of Physics, Bharathidasan University, Tiruchirappalli 620024, India
[4]School of Mathematics and Computer Science, Shanxi Normal University, Linfen 041004, China

Corresponding author: Guisheng Zhai (zhai@shibaura-it.ac.jp)

This work was supported by the Shibaura Institute of Technology, Japan.

**ABSTRACT** In this paper, we investigate sampled-data stabilization of memristor nonlinearity in Chua's circuits. The system stability pertaining to its switching nonlinearity covers two situations of flux thresholds. Through the stability analysis, the multistability characteristic is proved by its periodic invariant stable line. Moreover, the dynamical features of the considered system are examined in details by numerical and corresponding simulated experiments. Several statistical and analytical characteristic methods are used to confirm the existence of chaotic attractors. With the help of Lyapunov stability theory, new sufficient conditions are formulated using the linear matrix inequality (LMI) method to ensure robust stability and stabilization of closed-loop systems. Finally, we present a numerical example to ascertain the validity of the theoretical results obtained.

**INDEX TERMS** Chua's circuits, Lyapunov stability, linear matrix inequality (LMI), memristor, sampled-data control.

## I. INTRODUCTION

A memristor, i.e., a fourth-order basic passive circuit, was theoretically discovered by Chua in 1972 [1], while its existence was experimentally proved in 2008 [2]. Today, memristors have received great attention [3]–[6]. The theory of memristor has been developed based on electronically configurable simple elements made up of molecular-based logic gates by a research team in HP company, working together with the University of California [7]–[9]. Following the HP team's experimental proof of memristor elements by using CMOS nanoscale crossbars of electronic logic (2004), hysteric resistor crossbars were developed in 2005 [10]. Furthermore, they developed self-organized computation with an unreliable, memristive nano device [2], [10], [11]. The general working principles of a memristor component are like a simple switch (on/off) where it switches from a low resistive state to a high resistive state and vice versa. The switching principle of the memristor opens a second threshold voltage, and the device breaks well beyond either of the threshold voltages [12]. Later, HP merged the nano-ionics with Chua's concept [13], [14]. The term memristor was reused (also memristive system) in the experimental realization. Many research articles on the topic of memristors and memristive systems are available in the literature [13].

Many aspects of memristor-based systems and their dynamics have been studied, e.g. the memory properties, synaptic behaviours, and pinched $v - i$ characteristics curve, and the associated influence in many science and engineering areas have been reported [2], [3], [7]–[15]. In recent years, researchers have also investigated the memristive properties in various domains, including neuromorphic studies, fuzzy logic, artificial intelligence as well as in cellular neural networks, and others [14], [16]–[20]. In this paper, a memristive based Chua's family oscillator is considered [3]. The piecewise nonlinear element of the Chua diode can be replaced by the memristive element, allowing the investigation on the associated dynamics. Real-time analogue

The associate editor coordinating the review of this manuscript and approving it for publication was Norbert Herencsar.

circuits can also be constructed for prediction. Furthermore, the chaotic attractor can be characterized by the Lyapunov exponent using the Rosenstein algorithm [15].

LPV (Linear parameter varying) control techniques have received attention from researchers in the control community in the context of both theoretical investigations and practical applications [21]–[24]. Several systems have been successfully modelled by linear systems with certain parameters that change over time. In addition, some nonlinear systems can be described in quasi-LPV form by appropriately translating some nonlinearities of the product of states and varying the relevant parameters [21], [25], [26]. In both instances, the LPV controllers can be easily computed using the linear matrix inequality (LMI) method. The resulting LMIs match the matrix of the state-space model of the system. This relationship helps the examination of the considered systems with uncertain parameters. In [22], [27], [28], the parameter-dependent conditions for the stability of linear systems with polytopic uncertainty were studied. The iterative procedure requires an initial state feedback gain matrix that stabilizes the system across the uncertainty polytope, and it is not easy to obtain this gain matrix.

On the other hand, input nonlinearities from real environments occur in realistic engineering applications, such as mechanical connections, piezoelectric transducers, servo motors, etc. The nonlinearity of the equipment input decreases the performance of the system; and in some serious cases, the closed-loop system becomes unstable. For this reason, input nonlinear control methods have been examined. To reduce the control cost associated with the memristive systems, it is essential to embed the system in a microprocessor with limited energy and computing power. This means that the sampled-data control scheme has to be established on the digital platform [29]–[34]. Therefore, it is crucial to formulate a sampled-data control scheme for memristive systems to reduce the controller update time. In sampled-data control, the measured closed-loop dynamics plays an important role during sampling [35]–[39]. However, few papers on the sampled-data control scheme for LPV systems are available [40]–[43]. Therefore, it is important to investigate the dynamic behaviours of uncertain memristive systems. Recently, state feedback sliding mode control of memristor-based Chua's circuits has been reported in [44]. To the best of the authors' knowledge, the existing published literature does not provide the results of sampled-data stabilization of LPV memristor-based Chua's circuits (MCCs), and this is the motivation of this article. Moreover in this manuscript, the considered system has peculiar and very interesting nonlinear characteristics nature i.e., non smooth boundary switching type [45], [46]. There is another important motivation which leads to coin few future works like to apply the MCCs in the FPAA [47], fractional order [48] and other memristor emulators based switching type nonlinear systems studies.

Specifically, a unique methodology is proposed and applied to MCCs with parameter uncertainties in this study, serving as a sampled-data technique for analysing the stabilization of Chua's circuits. Firstly, a linear time-invariant state-space model is established for MCCs. It indicates that the model is unstable and multi-layered. As such, the kinetic aspects of the considered model are studied in detail with numerical and detailed experimental investigations. Secondly, a sampled-data control scheme is designed for such uncertain MCCs. The results indicate that robust sampled-data stabilization is achieved for the MCCs, and the simulation results confirm the advantages and benefits of the proposed method.

| Notations | Descriptions |
|---|---|
| $\mathbb{R}^n$ | Euclidean space of $n$ dimensions |
| $\mathbb{R}^{m\times n}$ | Set of all $m \times n$ dimension real matrices |
| $I_n$ | An identity matrix with dimension $n$ |
| $\mathbb{X} > 0$ | $\mathbb{X}$ is symmetric and positive-definite |
| $\|\cdot\|$ | Euclidean norm in $\mathbb{R}^n$ |
| $-$ | Symmetric block in a symmetric matrix |
| $diag\{\cdot\}$ | Block-diagonal matrix |

## II. SYSTEM DESCRIPTION AND DYNAMICAL ANALYSIS

### A. SYSTEM DESCRIPTION

The memristor is the fourth fundamental passive component that directly relates to flux $\varphi$ and charge $q$ [13]. Recently, the use of memristor emulators in the field of machine learning and biological networks is emerging [14]. The connection between charge and flux is

$$i = W(\varphi)V, \text{ or } V = M(q)i \tag{1}$$

where $V = d\varphi/dt$ and $i = dq/dt$. Based on both relations, a memristor can be categorized as memristance (voltage controlled $W(\varphi)$) or memductance (current controlled $M(q)$), respectively. They are defined as

$$W(\varphi) = \frac{dq(\varphi)}{d\varphi} \geq 0 \text{ and } M(q) = \frac{d\varphi(q)}{dq} \geq 0. \tag{2}$$

Recently, researchers have noticed that two types of memristor emulator concepts can be used for nonlinearity analysis by replacing the classical nonlinear elements (piecewise cubic, tanh, negative impedance converter, etc.) of dynamical systems. Several articles related to memristor-based nonlinear dynamical systems are available in the literature [1], [3], [13], [44]. Different forms of the memristor emulator are available in the literature, for example, floating memristor emulator [49], memristive neural network [50], etc.

The main benefit of utilising this memristor is that it has a memory feature. This present study focuses on replacing the well-known piecewise nonlinearity (i.e., Chua's diode) with a memristor emulator, as shown in Fig. 1. The piecewise nonlinearity form can be written as

$$q(\varphi) = b\varphi + \frac{1}{2}(a-b)\big(|\varphi+1| - |\varphi-1|\big). \tag{3}$$

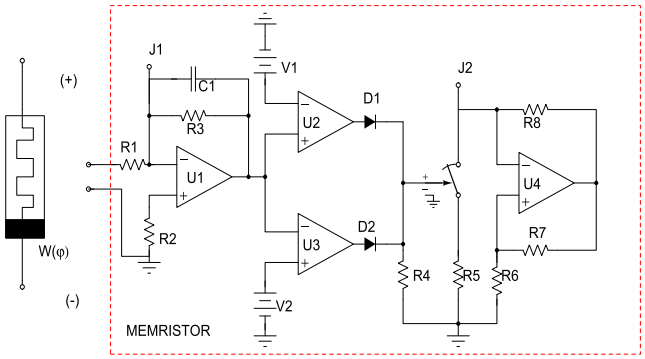


**FIGURE 1.** (red box): A circuit schematic of the memristor nonlinear element, which is equivalent to $W(\phi)$. The circuit is constructed using the Xcircuit software.

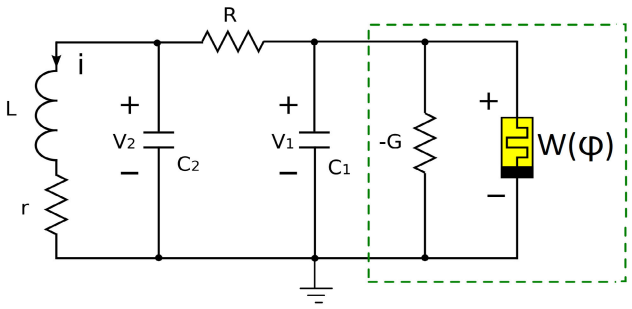


**FIGURE 2.** A flux-controlled MCC [3].

Initially proposed by Itoh and Chua [3], a memristive element can be characterized by the following monotone-increasing and piecewise linear function, and the equation (3) can be transformed into a memristor concept, i.e.,

$$W(\varphi) = \frac{dq(\varphi)}{d\varphi} = \begin{cases} a, & |\varphi| \le 1 \\ b, & |\varphi| > 1 \end{cases} \tag{4}$$

where the nonlinear slopes $a$ and $b$ are positive constants. Here the switching ON and OFF action achieved by an output pulse of a comparator is shown in Fig. 1. It compares the flux through the memristor between two reference levels, namely the breakdown points lying within $\pm 1$ flux unit. Notice that the negative impedance is included in the circuit. When the fluxes exceed the breakdown point, the resultant of the linear resistance and negative conductance, which are in parallel, is included in the circuit. Moreover, the flux achieved through the integrator circuit is shown in Fig. 1. By this action, the functional relationship between the flux and charge given in (1) is realized. More detailed description of this memristor model is given [45], [46], [51].

A memristive Chua's oscillator circuit with a monotone-increasing and piecewise linear memristor is presented in Fig. 2. Based on the Kirchhoff's law, the circuit equation can be written as

$$\begin{cases} C_1 \dfrac{dv_1(t)}{dt} = \dfrac{1}{R}(v_2(t) - v_1(t)) + Gv_1(t) - W(\varphi(t))v_1(t) \\ C_2 \dfrac{dv_2(t)}{dt} = \dfrac{-v_2(t) + v_1(t)}{R} - i(t) \\ L \dfrac{di(t)}{dt} = v_2(t) - ri(t) \\ \dfrac{d\varphi(t)}{dt} = v_1(t). \end{cases} \tag{5}$$

A real-time hardware experimental circuit can be composed for validating the numerical predictions. This complete circuit has been constructed through a circuit simulator (MULTISIM-student free version). The memristive emulator is constructed by using op-amp (U1 to U4) $\mu A741$ ICs, diodes (1N4007N) and the switching IC (MULTISIM: voltage-controlled-SPST-animated, Realtime Experiment: IC LM5017), as shown in Fig. 1. The switching IC operates according to the function in (4). The output of the variables $v_1$, $v_2$ and $i_L$ in the circuit are measured via the voltage across capacitors $C_1$ and $C_2$ and current via inductor $L$. Another state variable ($\phi(t)$) that a memristive component has measured by voltage across the capacitor $C_1$ in Fig. 1. The chaotic attractor can be realised using the following component values of the memristor emulator: $R_1 = R_4 = 10K\Omega$, $R_2 = R_3 = 100\text{K}\Omega$, $R_7 = R_8 = 2\text{K}\Omega$, $R_5 = 1450\Omega$, $R_6 = 1050\Omega$ and $C_1 = 2.2nF$. The Chua's circuit component values are $L = 18mH$, $r = 40\Omega$, $C_1 = 8nF$, $C_2 = 100nF$, $G = 1/R = 1800\Omega$. The chaotic attractor is shown in Fig. 3a. The present circuit is designed to confirm the presence/existence of the chaotic attractor in a real-time experiment. For the unavailability of the circuit component (switching IC), we perform the MULTISIM simulation instead of real-time hardware circuit. Moreover, we can also construct the same circuit by using field-programmable analog array (FPAA) platform [47]. It is very easy to implement, working in low bias voltages and the main advantage is the possibility of prototyping. The output can be seen in the oscilloscope. The phase portrait and its corresponding (Figs. 3b,c) time series of variables $v_1, v_2$ confirm the presence of chaos. Moreover, the period-doubling scenario can be seen visualizing the phase space (oscilloscope/simulation) by varying the $G = 1/R$ resistive component in the circuit. The experimentally observed chaotic attractor is further confirmed by using the $0-1$ test analysis.

### B. CHAOTIC BEHAVIOR ANALYSIS BY 0-1 TEST

In this section, the time series data are examined to confirm the chaotic oscillation by the '0-1' test. Gottwald *et al* [52] proposed a new method to classify the obtained time series is chaotic or periodic by simply calculating its asymptotic growth rate $K$. The growth rate $K$ of the time series confirms its dynamical content (periodic $K = 0$ and chaotic $K = 1$). The phase portrait of the translational coefficients $p, q$ partially confirms the nature of the time series (random walk: chaotic, smooth: periodic). In this analysis, the experimentally observed time series of the chaotic attractor is investigated.

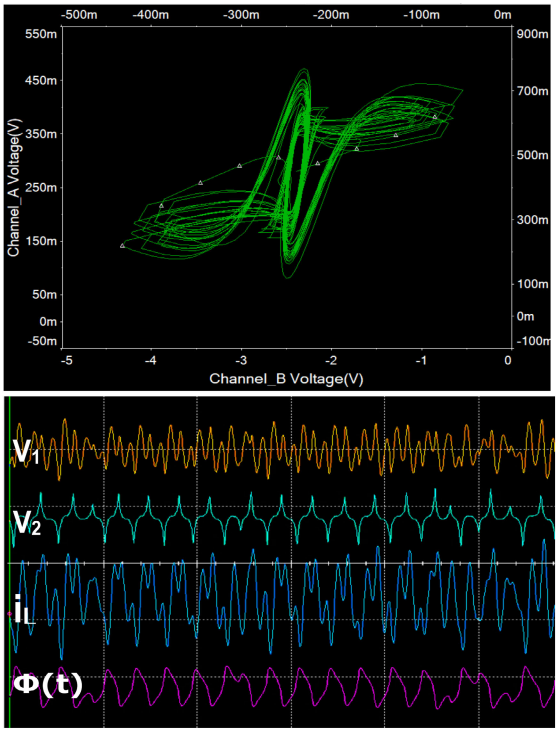


**FIGURE 3.** MultiSim circuit simulator: (a) Phase portrait in the voltages $v_1$ vs $v_2$ plane and (b) time series of the variables $v_1, v_2, i_L$ and $\phi(t)$ of the chaotic attractor of the proposed circuit.

Here, $x(j)$ is a given time series, and the dimensionless translational displacements are defined by

$$p(n) = \sum_{j=1}^{n} x(j)\ \cos(jc) \tag{6}$$
$$q(n) = \sum_{j=1}^{n} x(j)\ \sin(jc).$$

The arbitrarily chosen constant $c$ varies between $0 - \pi$. The time series considered has $2\times10^4$ data length. The calculation is carried out with 0.01 iterations. According to the concept of the $0-1$ test, the translational components $p-q$ visualizes the Brownian motion of the time series, which partially confirms the nature of chaotic motion, as shown in Fig. 4a. The mean square displacement $M(n)$ calculated from the translational components to find the diffusive behaviour ( for periodic, $M(n)$ is bounded; if it is chaotic, it linearly increases with time) of the given time series is shown in Fig. 4b. The mean square displacement $M(n)$ is calculated as

$$M(n) = \lim_{n\to\infty} \frac{1}{n} \sum_{j=1}^{n} \Big( [p_c(j+n) - p_c(j)]^2 + [q_c(j+n) - q_c(j)]^2 \Big). \tag{7}$$

The asymptotic growth rate $K$ calculated from the mean square displacement of the time series is

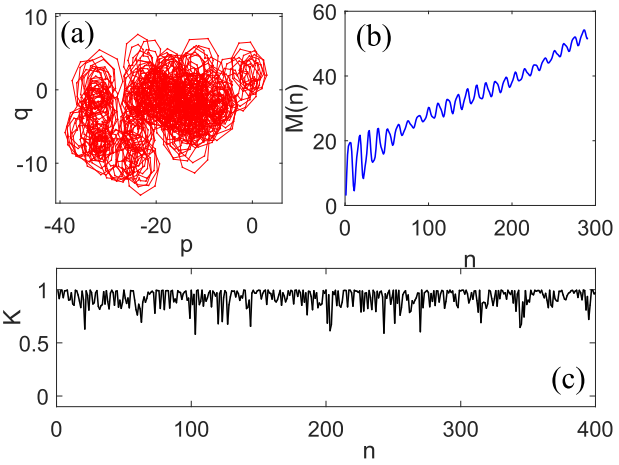


**FIGURE 4.** The 0-1 test: (a) phase portraits of translational components $(p-q)$ plane; (b) displacement $M(n)$; (c) asymptotic growth rate: $K$ of the given time series of the model.

derived by

$$K = \lim_{n\to\infty} \frac{\log M(n)}{\log n}. \tag{8}$$

The given time series data are evaluated with the above equation, and we obtain $K = 0.9941$ ($\sim 1$). It confirms the given time series has chaotic motion characteristics, as shown in Fig. 4c.

### C. SYSTEM STABILITY ANALYSIS

The circuit equation is normalized in [3]. Consider $x_1(t) = v_1(t)$, $x_2(t) = v_2(t)$, $x_3(t) = -i(t)$, $x_4(t) = \varphi(t)$, and the model parameters are refined as $\alpha = 1/C_1$, $\beta = 1/L$, $\rho = r/L, \epsilon = G, C_2 = 1$, and $R = 1$. Therefore, equation (5) can be transformed into

$$\begin{cases} \dfrac{dx_1}{dt} = \alpha(x_2 - x_1 + \epsilon x_1 - W(x_4)x_1) + u(t) \\ \dfrac{dx_2}{dt} = x_1 - x_2 + x_3 \\ \dfrac{dx_3}{dt} = -\beta x_2 - \rho x_3 \\ \dfrac{dx_4}{dt} = x_1. \end{cases} \tag{9}$$

The piecewise linear function $W(x_4)$ is given by

$$W(x_4) = \begin{cases} a, & |x_4| \le 1, \\ b, & |x_4| > 1. \end{cases} \tag{10}$$

The nature of the memristive nonlinearity depends only on its slope parameters $a, b$. The slope parameters are taken as positive values, $a, b > 0$. The other model parameters, $\alpha = 10$, $\beta = 13$, $\rho = 0.35$, $\epsilon = 1.5$ are fixed to find the chaotic attractor. Before that, the stability of the proposed dynamical model is studied. The circuit equation is transformed into a normalized form. Then, the equilibrium state is given by taking the initial conditions as $x_1, x_2,$

$x_3 = 0, x_4 = constant$), which corresponds to the $x_4$-axis. The Jacobian matrix $J$ at this equilibrium is given by

$$J = \begin{bmatrix} \alpha(-1+\epsilon - W(x_4)) & \alpha & 0 & 0 \\ 1 & -1 & 1 & 0 \\ 0 & -\beta & -\rho & 0 \\ 1 & 0 & 0 & 0 \end{bmatrix}.$$

Clearly, we have four eigenvalues of the matrix $J$. From the Jacobian matrix, the model stability depends on the flux correspondence variable $x_4$. This means that the model is always stable in the $x_4$ direction. This kind of equilibrium gives the 'periodic line invariant' type of stability of the model, and the model is always stable on the $x_4$ line [53]. We evaluate the above matrix with two different sides of variable $x_4$, and obtain the following set of eigenvalues.

- Case-I: For $|x_4| < 1$, we obtain $\lambda_{1,2} = -1.2115 \pm i2.7534$ and $\lambda_3 = 3.27$, $\lambda_4 = 0$. The model has a stable focus equilibrium point.
- Case-II: For $|x_4| > 1$, we obtain $\lambda_{1,2} = 0.0786 \pm i2.8454$ and $\lambda_3 = -4.5064$, $\lambda_4 = 0$. Thus, they are characterized by an unstable saddle-focus except for the zero eigenvalues. The model has unstable characteristics at $x_4$ =0.0; so this is avoided when calculating the eigenvalues.

To fix the circuit equation and the parameter values into the state-space format $x(t) = [x_1(t), x_2(t), x_3(t), x_4(t)]^T$, the initial value of the simulation model is selected as $x(0) = [-0.4, \ 0.8, \ 0.8, \ 5]^T$ for obtaining the chaotic attractor. To produce the model dynamics, the normalized equation is computed with the Runge Kutta $4^{th}$ algorithm with a fixed step size of 0.01. Fig. 5 depicts the phase portrait in (a) $x_1 - x_2$ plane; (c) the $x_1, x_2, x_4$ plane, along with the corresponding time series of (b,d) $x_1, x_4$ variables. The 3D plot shows the trajectories of the chaotic attractor. A number of measures confirm the nature of the chaotic attractor, as presented in the subsequent sections. While changing the control parameter $\alpha$, we can see the bifurcation by plotting the phase portraits and time series. The bifurcation of the present system is not possible because it has switching nonlinearity and nonsmooth boundaries. Therefore, we could not be able to plot the bifurcation by detecting peaks or Poincaré technique and any other way [45], [46].

The frequency component of the time series data for the chaotic attractor is numerically computed ($x_1$ variable) and observed. The calculation of the frequency component is complex in view of the raw time series data. The procedure is to convert the given signal data to the frequency domain. The discrete Fourier transform of the noisy signal ($x_1$) is formed by taking the $N$-point fast Fourier transform (FFT). The power spectrum, a measurement of the power at various frequencies, is $P = x_1 \times Conj(x_1)/N$. Then, plot the first $N/2 + 1$ points (the other $N/2 - 1$ points are redundant) on a meaningful frequency axis: $f = 1000(0 : N/2)/N$. If we plot between $P - f$ we can obtain the frequency content of variable $x_1$. Fig. 6 shows the frequency distribution with respect to the frequency content of variable $x_1$. The proposed dynamical model is of a multistability nature. The model goes

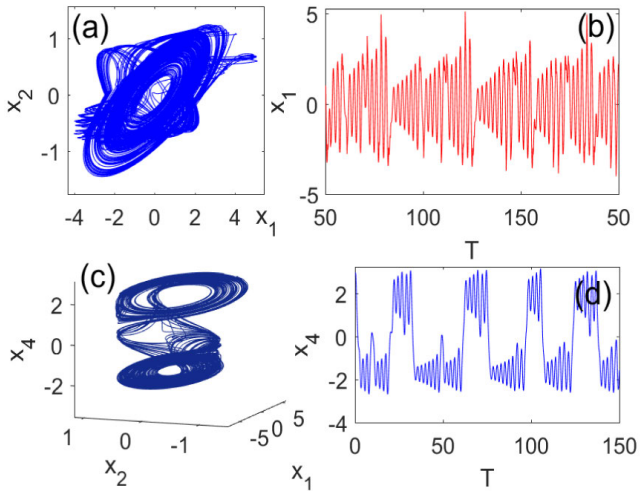


**FIGURE 5.** Numerically computed phase portrait in 2D: (a) $x_1 - x_2$ plane, and in 3D: (c) $x_1, x_2, x_4$ plane and the corresponding time series of (b,d) $x_1, x_4$ variables.

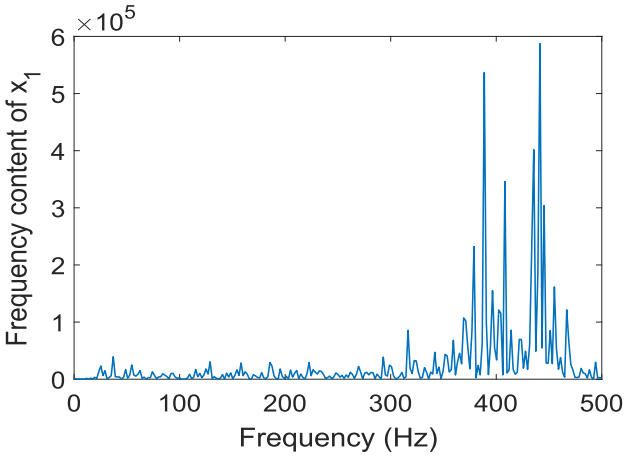


**FIGURE 6.** Numerically computed frequency distribution with respect to the frequency content of variable $x_1$. The broadband nature of the spectrum confirms the chaotic behaviour.

to infinity with respect to certain parameter sets. Therefore, the calculation of the bifurcation and its corresponding Lyapunov exponent is challenging. However, the confirmation of chaos can be achieved by calculating the Lyapunov exponent via its corresponding time series.

### D. LYAPUNOV EXPONENT

Rosenstein [15] developed a concept to find the maximal Lyapunov exponent (LE) in a time series, especially in a small data set. This method is robust, fast and easy to perform. It gives reliable results for detecting the dimension estimates of the time series. According to the Rosenstein approach, the phase portrait is (re)constructed $n$-dimensionally with the given time series $x(t)$ with its corresponding arbitrarily chosen delay ($\tau$) co-ordinates by $x(t), x(t+\tau), \cdots, x(t+[n-1]\tau)$. The initial difference between the original and its reconstructed trajectories

(nearest neighbours) is located at the initial point of the original trajectory as $(x(t_0), x(t_0+\tau), \cdots, x(t_0+[n-1]\tau))$. The difference of the two trajectories is denoted as $L(t_0)$ and that of the next iteration is denoted as $L'(t_1)$, which is evolved in length. The length element is propagated through the attractor for a time short enough so that only small-scale attractor structure is likely to be examined. For the next iteration of the trajectories (new points), the LE should satisfy the following two conditions: (i) the separation between the original and constructed trajectories (the nearest neighbour $L'(t_1)$) is small from its evolved fiducial point; (ii) the angular separation between the evolved replacement points (elements) is also small. If there are no adequate points, then retain the points that are being used. This calculation of this procedure is repeated until the fiducial trajectory has traversed the entire data set. The Lyapunov exponent is

$$\lambda = \frac{1}{t_n - t_0} \sum_{k=1}^{n} \log_2 \frac{L'(t_k)}{L(t_k - 1)}. \tag{11}$$

Here $n$ represents the number of replacement steps. If there is a fixed evolution between the replacement and time step, $\Delta = t_{k+1} - t_k$ is constant. The key advantage of this method to obtain LE $\lambda$ pertaining to a noise-free large amount of data set is that the procedure always provides replacement vectors of infinitesimal magnitude with no orientation error. Through this method, the obtained time series of $x_2$ is taken into account. The calculated LE is shown in Fig. 7. The top panel is considered time series, while the phase space reconstructed by the delay value of $\tau$ =770 is shown in the bottom left graph. The average divergence and convergence plot of the time series with various delay values is shown in the bottom right graph. The average of these values is LE, and the LE of this example is $\lambda$ =0.2580, which represents the nature of chaos. The periodicity and chaotic characteristics are confirmed via the maximal LE of its negative and positive values. Limitation of the study: For a very low number of data set, it is very hard to find the average divergence because the reconstructed attractor is not possible to visualize. Moreover, when we have different physical situations, a time series like periodic, chaotic, and quasiperiodic differentiation is possible when finding the mean of the average divergence instead of plotting the slope value. It also very sensitive to the initial conditions and optimized parameters [54].

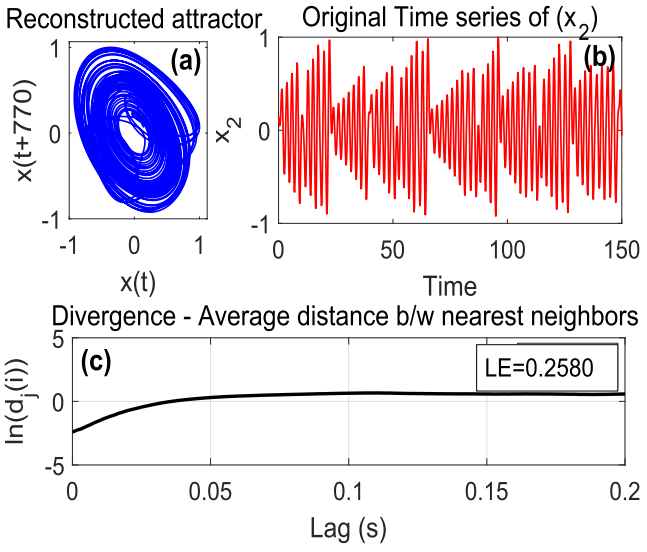


**FIGURE 7.** Numerically computed maximum Lyapunov exponent for the given time series.(a) The original time series, (b) phase space reconstruction, (c) average divergence.

## III. SAMPLED-DATA STABILIZATION

In this section, we consider the following MCC model with switching modes,

$$\dot{x}(t) = \mathcal{A}_{\sigma(t)}x(t) + \mathcal{B}_{\sigma(t)}u(t), \tag{12}$$

where

$$\mathcal{A}_{\sigma(t)} = \begin{bmatrix} \alpha(-1+\epsilon - W(w)) & \alpha & 0 & 0 \\ 1 & -1 & 1 & 0 \\ 0 & -\beta & -\rho & 0 \\ 1 & 0 & 0 & 0 \end{bmatrix},$$
$$\mathcal{B}_{\sigma(t)} = \begin{bmatrix} 1 & 0 & 0 & 0 \end{bmatrix}^T.$$

Based on the relation of memristor in (4), $x_4(t)$ is designed to carry out the switching between the following two modes

$$\dot{x}(t) = \begin{cases} \mathcal{A}_1 x(t) + \mathcal{B}_1 u(t), & |x_4(t)| \le 1, \\ \mathcal{A}_2 x(t) + \mathcal{B}_2 u(t), & |x_4(t)| > 1, \end{cases} \tag{13}$$

where

$$\mathcal{A}_1 = \begin{bmatrix} -\alpha + \alpha\epsilon - \alpha a & \alpha & 0 & 0 \\ 1 & -1 & 1 & 0 \\ 0 & -\beta & -\rho & 0 \\ 1 & 0 & 0 & 0 \end{bmatrix},$$
$$\mathcal{A}_2 = \begin{bmatrix} -\alpha + \alpha\epsilon - \alpha b & \alpha & 0 & 0 \\ 1 & -1 & 1 & 0 \\ 0 & -\beta & -\rho & 0 \\ 1 & 0 & 0 & 0 \end{bmatrix},$$
$$\mathcal{B}_1 = \mathcal{B}_2 = \begin{bmatrix} 1 & 0 & 0 & 0 \end{bmatrix}^T,$$

and the parameters $a$, $b$ are all positive constant values. The model can be further represented as a linear uncertain system

$$\dot{x}(t) = \mathcal{A}(\theta)x(t) + \mathcal{B}(\theta)u(t), \tag{14}$$

with the following rule

$$\theta_1 = \begin{cases} 1, & |x_4(t)| \le 1, \\ 0, & |x_4(t)| > 1, \end{cases} \qquad \theta_2 = 1 - \theta_1.$$

The state space matrices $\mathcal{A}(\theta)$ and $\mathcal{B}(\theta)$ are subject to real parameter uncertainty $\theta_i$, and obey the real convex polytopic model, i.e. $[\mathcal{A}(\theta) \quad \mathcal{B}(\theta)] \in \Omega$, where

$$\Omega = \left\{ [\mathcal{A}(\theta)\ \mathcal{B}(\theta)] := \sum_{i=1}^{2} \theta_i [\mathcal{A}_i\ \mathcal{B}_i],\ \theta_i \ge 0,\ \sum_{i=1}^{2} \theta_i = 1 \right\}. \tag{15}$$

### A. FORMULATION FOR SAMPLED-DATA CONTROL

Model (14) is designed as a continuous-time system. Its control input consists of a series of delays. The LMI-based sufficient conditions with respect to the model are derived using a descriptive method, which is a feedback confirmation time delay system. If the distance between successive sampling times is not greater than the preselected $h > 0$, the LMIs can be performed. The necessary and sufficient condition with respect to continuous-time state feedback stabilization is yielded when $h \to 0$. Consider the piecewise constant control function $u(t) = u(t_k),\ t_k \le t < t_{k+1}$, where $\lim_{k\to\infty} t_k = \infty$ and a series of sampling times $0 = t_0 < t_1 < \cdots < t_k < \cdots$, and assume that $h \in \mathbb{R}$ $(h > 0)$ and $t_{k+1} - t_k \le h,\ \forall k \ge 0$.

Corresponding to the sampled-data control principle, with the definition of $h(t) = t - t_k$ for $t \in [t_k, t_{k+1})$, the controller (14) becomes

$$u(t) = \mathcal{K}x(t - h(t)),\ t \in [t_k, t_{k+1}), \tag{16}$$

where $\mathcal{K}$ is the control gain to be determined. The closed-loop model under the above sampled-data control principle (16) becomes

$$\dot{x}(t) = \sum_{i=1}^{2} \theta_i[\mathcal{A}_i x(t) + \mathcal{B}_i \mathcal{K} x(t - h(t))]. \tag{17}$$

*Definition 1: Model* (14) *with* $u(t) = 0$ *is said to be robustly stable if the equilibrium solution* $x(t) = 0$ *is globally asymptotically stable for all* $[\mathcal{A}(\theta)\ \mathcal{B}(\theta)] \in \Omega$. *Model* (14) *is said to be robustly stabilizable via sampled-data controller if there exists a linear state feedback* (16) *such that the closed-loop model* (17) *is robustly stabilizable for all* $[\mathcal{A}(\theta)\ \mathcal{B}(\theta)] \in \Omega$.

To derive the main results, we state the following lemmas.

*Lemma 1 [55]: For positive definite matrix* $\mathcal{M} \in \mathbb{R}^{n\times n}$, *scalar* $\epsilon > 0$, *vector function* $x : [0, \epsilon] \to \mathbb{R}^n$ *such that the integrations concerned are well-defined,*

$$\left[\int_0^\epsilon x(s)ds\right]^T \mathcal{M}\left[\int_0^\epsilon x(s)ds\right] \le \epsilon \int_0^\epsilon x^T(s)\,\mathcal{M}x(s)ds.$$

*Lemma 2 [55]: Let* $f_1 > 0, f_2 > 0, \ldots, f_N > 0 : \mathbb{R}^m \mapsto \mathbb{R}$ *have positive values in an open subset* $\mathcal{D} \in \mathbb{R}^m$. *Then, the reciprocally convex combination of* $f_i$ *over set* $\mathcal{D}$ *satisfies*

$$\min_{\{\alpha_i|\alpha_i>0, \sum_i \alpha_i = 1\}} \sum_i \frac{1}{\alpha_i} f_i(t) = \sum_i f_i(t) + \max_{g_{ij}(t)} \sum_{i\ne j} g_{ij}(t)$$

*subject to*

$$\left\{g_{ij} : \mathbb{R}^m \mapsto \mathbb{R}, g_{ji}(t) = g_{ij}(t), \begin{bmatrix} f_i(t) & g_{ij}(t) \\ g_{ij}(t) & f_j(t) \end{bmatrix} \ge 0\right\}.$$

## IV. DESIGN CONDITIONS

The main purpose of this section is to derive new criteria for robustly stable analysis of model (17) with sampling time subject to uncertainties on the parameters.

*Theorem 1: For a given gain* $\mathcal{K}$ *and scalars* $0 < \delta < 1$ *and* $h > 0$, *model* (17) *is robustly stable if there exist positive-definite matrices* $\mathcal{P},\ \mathcal{Q},\ \mathcal{X},\ \mathcal{Y} \in \mathbb{R}^{n\times n}$, *appropriate dimensional matrices* $\mathcal{N}$ *and* $\mathcal{G}$ *such that the LMIs*

$$\Psi_i < 0,\ i = 1, 2, \tag{18}$$

*hold, where*

$$\Psi_i = \begin{bmatrix} \Psi_i(1,1) & \Psi_i(1,2) & 0 & \Psi_i(1,4) & \mathcal{N} \\ - & \Psi(2,2) & 0 & \mathcal{G}\mathcal{B}_i\mathcal{K} & 0 \\ - & - & \Psi(3,3) & 0 & 0 \\ - & - & - & \Psi(4,4) & \Psi(4,5) \\ - & - & - & - & \Psi(5,5) \end{bmatrix},$$

$$\Psi_i(1,1) = \mathcal{Q} + \mathcal{X} - \mathcal{Y} + \mathcal{G}\mathcal{A}_i + (\mathcal{G}\mathcal{A}_i)^T,$$
$$\Psi_i(1,2) = \mathcal{P} - \mathcal{G} + (\mathcal{G}\mathcal{A}_i)^T,\ \Psi_i(1,4) = \mathcal{Y} - \mathcal{N}^T + \mathcal{G}\mathcal{B}_i\mathcal{K},$$
$$\Psi(2,2) = h^2\mathcal{Y} - \mathcal{G} - \mathcal{G}^T,\ \Psi(3,3) = -(1-\delta)\mathcal{X},$$
$$\Psi(4,4) = -2\mathcal{Y} + \mathcal{N} + \mathcal{N}^T,\ \Psi(4,5) = \mathcal{Y}^T - \mathcal{N}^T,$$
$$\Psi(5,5) = -\mathcal{Q} - \mathcal{Y}.$$

*Proof:* Construct the following LKF candidate for model (17)

$$\begin{aligned} V(t) = {} & x^T(t)\mathcal{P}x(t) + \int_{t-h}^{t} x^T(s)\mathcal{Q}x(s)ds \\ & + \int_{t-\delta h(t)}^{t} x^T(s)\mathcal{X}x(s)ds \\ & + h\int_h^0 \int_{t+\theta}^{t} \dot{x}^T(s)\mathcal{Y}\dot{x}(s)ds d\theta, \end{aligned} \tag{19}$$

where $\delta$ is a constant satisfying $0 < \delta < 1$. Taking derivative of LKF in (19), we have

$$\begin{aligned} \dot{V}(t) = {} & 2x^T(t)\mathcal{P}\dot{x}(t) + x^T(t)\mathcal{Q}x(t) - x^T(t-h)\mathcal{Q}x(t-h) \\ & + x^T(t)\mathcal{X}x(t) - (1-\delta)x^T(t-\delta h(t))\mathcal{X}x(t-\delta h(t)) \\ & + h^2\dot{x}^T(t)\mathcal{Y}\dot{x}(t) - h\int_{t-h}^{t} \dot{x}^T(s)\mathcal{Y}\dot{x}(s)ds. \end{aligned} \tag{20}$$

Applying Lemmas 1 and 2 to handle the integral term $-h\int_{t-h}^{t} \dot{x}^T(s)\mathcal{Y}\dot{x}(s)ds$, it results in

$$\begin{aligned} & -h\int_{t-h}^{t} \dot{x}^T(s)\mathcal{Y}\dot{x}(s)ds \\ & = -h\int_{t-h}^{t-h(t)} \dot{x}^T(s)\mathcal{Y}\dot{x}(s)ds - h\int_{t-h(t)}^{t} \dot{x}^T(s)\mathcal{Y}\dot{x}(s)ds \\ & \le -\frac{h}{h-h(t)}\left(\int_{t-h}^{t-h(t)} \dot{x}(s)ds\right)^T \mathcal{Y}\left(\int_{t-h}^{t-h(t)} \dot{x}(s)ds\right) \\ & \quad -\frac{h}{h(t)}\left(\int_{t-h(t)}^{t} \dot{x}(s)ds\right)^T \mathcal{Y}\left(\int_{t-h(t)}^{t} \dot{x}(s)ds\right) \\ & \le -[x(t-h(t)) - x(t-h)]^T\mathcal{Y}[x(t-h(t)) - x(t-h)] \\ & \quad -[x(t) - x(t-h(t))]^T\mathcal{Y}[x(t) - x(t-h(t))] \\ & \quad -2[x(t) - x(t-h(t))]^T\mathcal{N}[x(t-h(t)) - x(t-h)] \\ & = \begin{bmatrix} x(t) \\ x(t-h) \\ x(t-h(t)) \end{bmatrix}^T \begin{bmatrix} -\mathcal{Y} & \mathcal{N} & \mathcal{Y} - \mathcal{N}^T \\ - & -\mathcal{Y} & \mathcal{Y} - \mathcal{N} \\ - & - & -2\mathcal{Y} + \mathcal{N} + \mathcal{N}^T \end{bmatrix} \\ & \quad \times \begin{bmatrix} x(t) \\ x(t-h) \\ x(t-h(t)) \end{bmatrix}. \end{aligned} \tag{21}$$

On the other hand, for any matrix $\mathcal{G}$ with suitable dimensions, we have

$$\begin{aligned}0 &= 2[x^T(t)\mathcal{G} + \dot{x}^T(t)\mathcal{G}] \times [-\dot{x}(t) + \dot{x}(t)] \\ &= 2[x^T(t)\mathcal{G} + \dot{x}^T(t)\mathcal{G}] \times \big[ -\dot{x}(t) + \mathcal{A}_i x(t) \\ &\quad + \mathcal{B}_i \mathcal{K} x(t - h(t))\big] \\ &= -2x^T(t)\mathcal{G}\dot{x}(t) + 2x^T(t)\mathcal{G}\mathcal{A}_i x(t) \\ &\quad + 2x^T(t)\mathcal{G}\mathcal{B}_i\mathcal{K}x(t - h(t)) - 2\dot{x}^T(t)\mathcal{G}\dot{x}(t) \\ &\quad + 2\dot{x}^T(t)\mathcal{G}\mathcal{A}_i x(t) + 2\dot{x}^T(t)\mathcal{G}\mathcal{B}_i\mathcal{K}x(t - h(t)). \quad (22)\end{aligned}$$

Combining (20)–(22), we obtain

$$\begin{aligned}\dot{V}(t) &\le 2x^T(t)\mathcal{P}\dot{x}(t) + x^T(t)\mathcal{Q}x(t) - x^T(t-h)\mathcal{Q}x(t-h) \\ &\quad + x^T(t)\mathcal{X}x(t) - (1-\delta)x^T(t-\delta h(t))\mathcal{X}x(t-\delta h(t)) \\ &\quad + \begin{bmatrix} x(t) \\ x(t-h) \\ x(t-h(t)) \end{bmatrix}^T \begin{bmatrix} -\mathcal{Y} & \mathcal{N} & \mathcal{Y} - \mathcal{N}^{\mathcal{T}} \\ - & -\mathcal{Y} & \mathcal{Y} - \mathcal{N} \\ - & - & -2\mathcal{Y} + \mathcal{N} + \mathcal{N}^{\mathcal{T}} \end{bmatrix} \\ &\quad \times \begin{bmatrix} x(t) \\ x(t-h) \\ x(t-h(t)) \end{bmatrix} + h^2\dot{x}^T(t)Y\dot{x}(t) - 2x^T(t)G\dot{x}(t) \\ &\quad + 2x^T(t)\mathcal{G}\mathcal{A}_i x(t) + 2x^T(t)\mathcal{G}\mathcal{B}_i\mathcal{K}x(t-h(t)) \\ &\quad - 2\dot{x}^T(t)\mathcal{G}\dot{x}(t) + 2\dot{x}^T(t)\mathcal{G}\mathcal{A}_i x(t) \\ &\quad + 2\dot{x}^T(t)\mathcal{G}\mathcal{B}_i\mathcal{K}x(t-h(t)) \\ &\le \sum_{i=1}^{2} \theta_i \Big[ \Sigma^T(t)\Psi_i\Sigma(t) \Big], \quad (23)\end{aligned}$$

where $\Sigma(t) = \big[x^T(t)\, \dot{x}^T(t)\, x^T(t-\delta h(t))\, x^T(t-h(t))\, x^T(t-h)\big]^T$ and $\Psi_i$ is defined in (18). Obviously, if matrix inequalities $\Psi_i < 0$ hold, we have $\dot{V}(t) \le 0$, indicating that the closed-loop model (17) is robustly stable for all $[\mathcal{A}(\theta)\ \mathcal{B}(\theta)] \in \Omega$. This completes the proof. ■

Next, the controller design criteria are introduced based on the stability conditions described above. If the controller is unknown, Theorem 1 is no longer an LMI-based condition due to the product of $\mathcal{G}\mathcal{B}_i\mathcal{K}$. To solve this problem, we present the following theorem for obtaining the controller parameters.

*Theorem 2: For given scalars $0 < \delta < 1$ and $h > 0$, model (17) is robustly stabilizable if there exist symmetric positive-definite matrices $\overline{\mathcal{P}}$, $\overline{\mathcal{Q}}$, $\overline{\mathcal{X}}$, $\overline{\mathcal{Y}} \in \mathbb{R}^{n\times n}$, nonsingular matrix $\overline{\mathcal{G}}$ and appropriate dimensioned matrices $\overline{\mathcal{N}}$ and $\mathcal{H}$ such that the LMIs*

$$\overline{\Psi}_i < 0,\ i = 1, 2, \quad (24)$$

*hold, where*

$$\overline{\Psi}_i = \begin{bmatrix} \overline{\Psi}_i(1,1) & \overline{\Psi}_i(1,2) & 0 & \overline{\Psi}_i(1,4) & \overline{\mathcal{N}} \\ - & \overline{\Psi}(2,2) & 0 & \mathcal{B}_i\mathcal{H} & 0 \\ - & - & \overline{\Psi}(3,3) & 0 & 0 \\ - & - & - & \overline{\Psi}(4,4) & \overline{\Psi}(4,5) \\ - & - & - & - & \overline{\Psi}(5,5) \end{bmatrix},$$

$$\begin{aligned}&\overline{\Psi}_i(1,1) = \overline{\mathcal{Q}} + \overline{\mathcal{X}} - \overline{\mathcal{Y}} + \mathcal{A}_i\overline{\mathcal{G}} + \overline{\mathcal{G}}^{\mathcal{T}}\mathcal{A}_i^T, \\ &\overline{\Psi}_i(1,2) = \overline{\mathcal{P}} - \overline{\mathcal{G}} + \overline{\mathcal{G}}^{\mathcal{T}}\mathcal{A}_i^T,\ \overline{\Psi}_i(1,4) = \overline{\mathcal{Y}} - \overline{\mathcal{N}}^{\mathcal{T}} + \mathcal{B}_i\mathcal{H}, \\ &\overline{\Psi}(2,2) = h^2\overline{\mathcal{Y}} - \overline{\mathcal{G}} - \overline{\mathcal{G}}^{\mathcal{T}},\ \overline{\Psi}(3,3) = -(1-\delta)\overline{\mathcal{X}}, \\ &\overline{\Psi}(4,4) = -2\overline{\mathcal{Y}} + \overline{\mathcal{N}} + \overline{\mathcal{N}}^{\mathcal{T}},\ \overline{\Psi}(4,5) = \overline{\mathcal{Y}}^{\mathcal{T}} - \overline{\mathcal{N}}^{\mathcal{T}}, \\ &\overline{\Psi}(5,5) = -\overline{\mathcal{Q}} - \overline{\mathcal{Y}}.\end{aligned}$$

*When the condition is satisfied, the control gain matrix is calculated by $\mathcal{K} = \mathcal{H}\overline{\mathcal{G}}^{-1}$.*

*Proof:* Define $\mathcal{K}\overline{\mathcal{G}} = \mathcal{H}$, $\overline{\mathcal{G}} = \mathcal{G}^{-1}$, $\Lambda = \mathrm{diag}\{\overbrace{\overline{\mathcal{G}}, \cdots, \overline{\mathcal{G}}}^{5\ times}\}$, and moreover,

$$\begin{aligned}&\overline{\mathcal{P}} = \overline{\mathcal{G}}\mathcal{P}\overline{\mathcal{G}},\ \overline{\mathcal{Q}} = \overline{\mathcal{G}}\mathcal{Q}\overline{\mathcal{G}},\ \overline{\mathcal{X}} = \overline{\mathcal{G}}\mathcal{X}\overline{\mathcal{G}}, \\ &\overline{\mathcal{Y}} = \overline{\mathcal{G}}\mathcal{Y}\overline{\mathcal{G}},\ \overline{\mathcal{N}} = \overline{\mathcal{G}}\mathcal{N}\overline{\mathcal{G}}.\end{aligned}$$

Then, pre- and post-multiplying (18) by $\Lambda$ and its transpose, respectively, we obtain the LMI (24). This completes the proof. ■

## V. SIMULATIONS

An example is presented to demonstrate the effectiveness of the proposed MCC model. Consider the following linear uncertain system:

$$\dot{x}(t) = \sum_{i=1}^{2} \theta_i[\mathcal{A}_i x(t) + \mathcal{B}_i u(t)], \quad (25)$$

where

$$\mathcal{A}_1 = \begin{bmatrix} -\alpha + \alpha\epsilon - \alpha a & \alpha & 0 & 0 \\ 1 & -1 & 1 & 0 \\ 0 & -\beta & -\rho & 0 \\ 1 & 0 & 0 & 0 \end{bmatrix},$$

$$\mathcal{A}_2 = \begin{bmatrix} -\alpha + \alpha\epsilon - \alpha b & \alpha & 0 & 0 \\ 1 & -1 & 1 & 0 \\ 0 & -\beta & -\rho & 0 \\ 1 & 0 & 0 & 0 \end{bmatrix},$$

$$\mathcal{B}_1 = \mathcal{B}_2 = \begin{bmatrix} 1 & 0 & 0 & 0 \end{bmatrix}^T.$$

Using the parameters defined in Section II-C, we have

$$\mathcal{A}_1 = \begin{bmatrix} 4.00 & 10.00 & 0 & 0 \\ 1.00 & -1.00 & -1.00 & 0 \\ 0 & -13.00 & -0.35 & 0 \\ 1.00 & 0 & 0 & 0 \end{bmatrix},$$

$$\mathcal{A}_2 = \begin{bmatrix} -3.00 & 10.00 & 0 & 0 \\ 1.00 & -1.00 & -1.00 & 0 \\ 0 & -13.00 & -0.35 & 0 \\ 1.00 & 0 & 0 & 0 \end{bmatrix}.$$

The sampled-data controller is formed as

$$u(t) = \mathcal{K}x(t_k),\ t \in [t_k, t_{k+1}).$$

According to LMI (24), when $a = 0.3$, $b = 0.8$, $\delta = 0.02$ and $h = 0.01$, the control gain obtained via the LMI Control Toolbox of MATLAB is

$$\mathcal{K} = \begin{bmatrix} -24.8999 & -122.0342 & 33.8704 & 0.1689 \end{bmatrix}.$$

With the help of the gain matrix $\mathcal{K}$, the simulation result of the closed-loop system is displayed in Figs. 8-9.

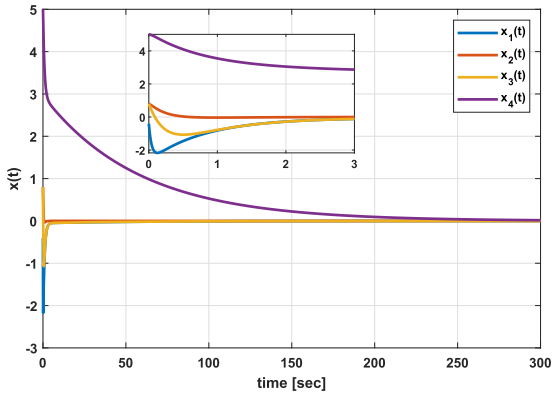


**FIGURE 8.** State response of the closed-loop MCC model.

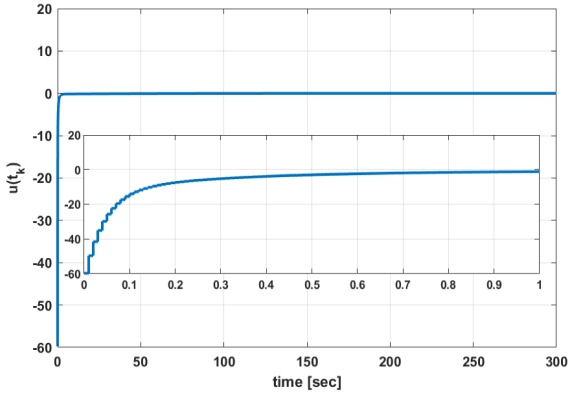


**FIGURE 9.** Control response of the MCC model.

It is observed from these figures that the state responses of the system are well stabilized via the proposed sampled-data control. This indicates that the closed-loop system (17) is asymptotically stable under the same initial states as $x(0) = [-0.4,\ 0.8,\ 0.8,\ 5]^T$.

## VI. CONCLUSION

Based on a sampled-data control method, the MCC models with parameter uncertainties have been studied in this paper. Initially, an uncertain MCC model is described as a linear uncertainty system based on the function of the memristor. The existence of a minimum execution time has been derived for the execution of the sampled-data control signals. The proposed scheme can be used to handle real-time applications of MCC models. Finally, robust sampled-data stabilization has also been achieved throughout the circuits, and the simulation results confirm the corresponding benefits.

One disadvantage of the present work is the existence of possible bifurcation plot because the considered system equation has switching nonlinearities which create multistability. It is noted that we can see the bifurcation by visualizing the phase space plot which is shown in Fig. 5. In the future, we plan to extend this work by using a fractional-order platform [48].

## REFERENCES

[1] L. Chua, "Memristor—The missing circuit element," *IEEE Trans. Circuit Theory*, vol. 18, no. 5, pp. 507–519, Sep. 1971.
[2] D. B. Strukov, G. S. Snider, D. R. Stewart, and R. S. Williams, "The missing memristor found," *Nature*, vol. 453, no. 7191, pp. 80–83, May 2008.
[3] M. Itoh and L. O. Chua, "Memristor oscillators," *Int. J. Bifurcation Chaos*, vol. 18, no. 11, pp. 3183–3206, Nov. 2008.
[4] D. Wang, Z. Hu, X. Yu, and J. Yu, "A PWL model of memristor and its application example," in *Proc. Int. Conf. Commun., Circuits Syst.*, Jul. 2009, pp. 932–934.
[5] F. Z. Wang, N. Helian, S. Wu, M.-G. Lim, Y. Guo, and M. A. Parker, "Delayed switching in memristors and memristive systems," *IEEE Electron Device Lett.*, vol. 31, no. 7, pp. 755–757, Jul. 2010.
[6] S. Ding, Z. Wang, N. Rong, and H. Zhang, "Exponential stabilization of memristive neural networks via saturating sampled-data control," *IEEE Trans. Cybern.*, vol. 47, no. 10, pp. 3027–3039, Oct. 2017.
[7] C. D. Schuman, T. E. Potok, R. M. Patton, J. D. Birdwell, M. E. Dean, G. S. Rose, and J. S. Plank, "A survey of neuromorphic computing and neural networks in hardware," 2017, *arXiv:1705.06963*. [Online]. Available: http://arxiv.org/abs/1705.06963
[8] P. J. Kuekes, R. S. Williams, and J. R. Heath, "Molecular wire crossbar memory," U.S. Patent 6 128 214, Oct. 3, 2000,
[9] J. R. Heath, C. P. Collier, G. Mattersteig, F. M. Raymo, J. F. Stoddart, and E. Wong, "Electrically addressable volatile non-volatile molecular-based switching devices," U.S. Patent 6 198 655, Mar. 6, 2001.
[10] G. Snider, "Computing with hysteretic resistor crossbars," *Appl. Phys. A, Solids Surf.*, vol. 80, no. 6, pp. 1165–1172, Mar. 2005.
[11] G. Snider, P. Kuekes, and R. S. Williams, "CMOS-like logic in defective, nanoscale crossbars," *Nanotechnology*, vol. 15, no. 8, p. 881, 2004.
[12] J. J. Yang, M.-X. Zhang, J. P. Strachan, F. Miao, M. D. Pickett, R. D. Kelley, G. Medeiros-Ribeiro, and R. S. Williams, "High switching endurance in TaOx memristive devices," *Appl. Phys. Lett.*, vol. 97, no. 23, Dec. 2010, Art. no. 232102.
[13] A. K. Maan, D. A. Jayadevi, and A. P. James, "A survey of memristive threshold logic circuits," *IEEE Trans. Neural Netw. Learn. Syst.*, vol. 28, no. 8, pp. 1734–1746, Aug. 2017.
[14] A. L. Despotuli and A. V. Andreeva, "Nanoionics: New materials and supercapacitors," *Nanotechnologies Russia*, vol. 5, nos. 7–8, pp. 506–520, Aug. 2010.
[15] M. T. Rosenstein, J. J. Collins, and C. J. De Luca, "A practical method for calculating largest Lyapunov exponents from small data sets," *Phys. D, Nonlinear Phenomena*, vol. 65, nos. 1–2, pp. 117–134, May 1993.
[16] T. Serrano-Gotarredona, T. Masquelier, T. Prodromakis, G. Indiveri, and B. Linares-Barranco, "STDP and STDP variations with memristors for spiking neuromorphic learning systems," *Frontiers Neurosci.*, vol. 7, p. 23, Feb. 2013.
[17] M. Klimo and O. Such, "Memristors can implement fuzzy logic," 2011, *arXiv:1110.2074*. [Online]. Available: http://arxiv.org/abs/1110.2074
[18] J. H. Yoon, Z. Wang, K. M. Kim, H. Wu, V. Ravichandran, Q. Xia, C. S. Hwang, and J. J. Yang, "An artificial nociceptor based on a diffusive memristor," *Nature Commun.*, vol. 9, no. 1, pp. 1–9, Dec. 2018.
[19] E. Lehtonen and M. Laiho, "CNN using memristors for neighborhood connections," in *Proc. 12th Int. Workshop Cellular Nanosc. Netw. Their Appl. (CNNA)*, Feb. 2010, pp. 1–4.
[20] S. Duan, X. Hu, Z. Dong, L. Wang, and P. Mazumder, "Memristor-based cellular Nonlinear/Neural network: Design, analysis, and applications," *IEEE Trans. Neural Netw. Learn. Syst.*, vol. 26, no. 6, pp. 1202–1213, Jun. 2015.
[21] Y. Huang and A. Jadbabaie, "Nonlinear $H_\infty$ control: An enhanced quasi-LPV approach," *IFAC Proc. Volumes*, vol. 32, no. 2, pp. 2754–2759, Jul. 1999.
[22] G. Zhai, H. Lin, and P. J. Antsaklis, "Quadratic stabilizability of switched linear systems with polytopic uncertainties," *Int. J. Control*, vol. 76, no. 7, pp. 747–753, Jan. 2003.
[23] E. Fridman and U. Shaked, "Parameter dependent stability and stabilization of uncertain time-delay systems," *IEEE Trans. Autom. Control*, vol. 48, no. 5, pp. 861–866, May 2003.
[24] G. Zhai, B. Hu, K. Yasuda, and A. N. Michel, "Disturbance attenuation properties of time-controlled switched systems," *J. Franklin Inst.*, vol. 338, no. 7, pp. 765–779, Nov. 2001.
[25] Y. Chang, G. Zhai, B. Fu, and L. Xiong, "Quadratic stabilization of switched uncertain linear systems: A convex combination approach," *IEEE/CAA J. Automatica Sinica*, vol. 6, no. 5, pp. 1116–1126, Sep. 2019.

[26] Y. Chang, G. Zhai, L. Xiong, and B. Fu, "Global quadratic stabilization in probability for switched linear stochastic systems," *IEEE Access*, vol. 8, pp. 103610–103618, 2020.
[27] D. Peaucelle, D. Arzelier, O. Bachelier, and J. Bernussou, "A new robust D-stability condition for real convex polytopic uncertainty," *Syst. Control Lett.*, vol. 40, no. 1, pp. 21–30, 2000.
[28] P. Gahinet, P. Apkarian, and M. Chilali, "Affine parameter-dependent Lyapunov functions and real parametric uncertainty," *IEEE Trans. Autom. Control*, vol. 41, no. 3, pp. 436–442, Mar. 1996.
[29] J. Mao, Z. Xiang, G. Zhai, and J. Guo, "Adaptive practical stabilization of a class of uncertain nonlinear systems via sampled-data control," *Nonlinear Dyn.*, vol. 92, no. 4, pp. 1679–1694, Jun. 2018.
[30] J. Mao, Z. Xiang, and G. Zhai, "Sampled-data control of a class of switched nonlinear systems under asynchronous switching," *J. Franklin Inst.*, vol. 356, no. 4, pp. 1924–1943, Mar. 2019.
[31] W. Zhang, Q.-L. Han, Y. Tang, and Y. Liu, "Sampled-data control for a class of linear time-varying systems," *Automatica*, vol. 103, pp. 126–134, May 2019.
[32] C. Hua, S. Wu, and X. Guan, "Stabilization of T-S fuzzy system with time delay under sampled-data control using a new looped-functional," *IEEE Trans. Fuzzy Syst.*, vol. 28, no. 2, pp. 400–407, Feb. 2020.
[33] N. Gunasekaran and Y. H. Joo, "Robust sampled-data fuzzy control for nonlinear systems and its applications: Free-weight matrix method," *IEEE Trans. Fuzzy Syst.*, vol. 27, no. 11, pp. 2130–2139, Nov. 2019.
[34] N. Gunasekaran, G. Zhai, and Q. Yu, "Sampled-data synchronization of delayed multi-agent networks and its application to coupled circuit," *Neurocomputing*, vol. 413, pp. 499–511, Nov. 2020.
[35] Z.-P. Wang, H.-N. Wu, and H.-X. Li, "Sampled-data fuzzy control for nonlinear coupled parabolic PDE-ODE systems," *IEEE Trans. Cybern.*, vol. 47, no. 9, pp. 2603–2615, Sep. 2017.
[36] Z.-P. Wang and H.-N. Wu, "On fuzzy sampled-data control of chaotic systems via a time-dependent Lyapunov functional approach," *IEEE Trans. Cybern.*, vol. 45, no. 4, pp. 819–829, Apr. 2015.
[37] P. Muthukumar, S. Arunagirinathan, and S. Lakshmanan, "Nonfragile sampled-data control for uncertain networked control systems with additive time-varying delays," *IEEE Trans. Cybern.*, vol. 49, no. 4, pp. 1512–1523, Apr. 2019.
[38] X. Wang, J. H. Park, H. Yang, G. Zhao, and S. Zhong, "An improved fuzzy sampled-data control to stabilization of T–S fuzzy systems with state delays," *IEEE Trans. Cybern.*, vol. 50, no. 7, pp. 3125–3135, Jul. 2020.
[39] M. S. Ali, N. Gunasekaran, C. K. Ahn, and P. Shi, "Sampled-data stabilization for fuzzy genetic regulatory networks with leakage delays," *IEEE/ACM Trans. Comput. Biol. Bioinf.*, vol. 15, no. 1, pp. 271–285, Jan. 2018.
[40] S. Maalej, A. Kruszewski, and L. Belkoura, "Derivative-based sampled data control for continuous linear parameter varying system with unknown parameters," *J. Dyn. Syst., Meas., Control*, vol. 141, no. 8, Aug. 2019.
[41] S. Li, S. Jiang, and F. Pan, "Event-triggered fault detection for networked LPV systems," *Circuits, Syst., Signal Process.*, vol. 38, no. 7, pp. 2992–3019, Jul. 2019.
[42] J. M. Palma, C. F. Morais, and R. C. L. F. Oliveira, "$H_\infty$ control and filtering of discrete-time LPV systems exploring statistical information of the time-varying parameters," *J. Franklin Inst.*, vol. 357, no. 6, pp. 3835–3864, Apr. 2020.
[43] N. Gunasekaran and Y. H. Joo, "Stochastic sampled–data controller for T–S fuzzy chaotic systems and its applications," *IET Control Theory Appl.*, vol. 13, no. 12, pp. 1834–1843, Aug. 2019.
[44] Y. Xue, B.-C. Zheng, T. Li, and Y. Li, "Robust adaptive state feedback sliding-mode control of memristor-based Chua's systems with input nonlinearity," *Appl. Math. Comput.*, vol. 314, pp. 142–153, Dec. 2017.
[45] A. Ishaq Ahamed and M. Lakshmanan, "Nonsmooth bifurcations, transient hyperchaos and hyperchaotic beats in a memristive Murali–Lakshmanan–Chua circuit," *Int. J. Bifurcation Chaos*, vol. 23, no. 06, Jun. 2013, Art. no. 1350098.
[46] A. I. Ahamed and M. Lakshmanan, "Discontinuity induced hopf and Neimark–Sacker bifurcations in a memristive Murali–Lakshmanan–Chua circuit," *Int. J. Bifurcation Chaos*, vol. 27, no. 06, Jun. 2017, Art. no. 1730021.
[47] A. Silva-Juárez, E. Tlelo-Cuautle, L. G. de la Fraga, and R. Li, "FPAA-based implementation of fractional-order chaotic oscillators using first-order active filter blocks," *J. Adv. Res.*, vol. 25, pp. 77–85, Sep. 2020.
[48] C. Sánchez-López, V. H. Carbajal-Gómez, M. A. Carrasco-Aguilar, and I. Carro-Pérez, "Fractional-order memristor emulator circuits," *Complexity*, vol. 2018, May 2018, Art. no. 2806976.
[49] C. Sánchez-López, J. Mendoza-López, M. A. Carrasco-Aguilar, and C. Muñiz-Montero, "A floating analog memristor emulator circuit," *IEEE Trans. Circuits Syst. II, Exp. Briefs*, vol. 61, no. 5, pp. 309–313, May 2014.
[50] I. Carro-Pérez, C. Sánchez-López, and H. G. González-Hernández, "Experimental verification of a memristive neural network," *Nonlinear Dyn.*, vol. 93, no. 4, pp. 1823–1840, Sep. 2018.
[51] C. Du, L. Liu, S. Shi, and Y. Wei, "Multiple transient transitions behavior analysis of a double Memristor's hidden system and its circuit," *IEEE Access*, vol. 8, pp. 76642–76656, 2020.
[52] G. A. Gottwald and I. Melbourne, "On the implementation of the 0–1 test for chaos," *SIAM J. Appl. Dyn. Syst.*, vol. 8, no. 1, pp. 129–145, Jan. 2009.
[53] V. Varshney, S. Sabarathinam, A. Prasad, and K. Thamilmaran, "Infinite number of hidden attractors in memristor-based autonomous duffing oscillator," *Int. J. Bifurcation Chaos*, vol. 28, no. 01, Jan. 2018, Art. no. 1850013.
[54] V. H. Carbajal-Gomez, E. Tlelo-Cuautle, J. M. Muñoz-Pacheco, L. G. de la Fraga, C. Sanchez-Lopez, and F. V. Fernandez-Fernandez, "Optimization and CMOS design of chaotic oscillators robust to PVT variations: Invited," *Integration*, vol. 65, pp. 32–42, Mar. 2019.
[55] P. Park, J. W. Ko, and C. Jeong, "Reciprocally convex approach to stability of systems with time-varying delays," *Automatica*, vol. 47, no. 1, pp. 235–238, Jan. 2011.

**NALLAPPAN GUNASEKARAN** was born in 1987. He received the bachelor's degree from the Mahendra Arts and Science College, Namakkal, affiliated to Periyar University, Salem, India, in 2009, the master's degree in mathematics from the Jamal Mohamed College, affiliated to Bharathidasan University, Tiruchirappalli, India, in 2012, the M.Phil. degree in mathematics with specialized area of cryptography from Bharathidasan University, in 2013, and the Ph.D. degree in mathematics from Thiruvalluvar University, Vellore, India, in 2017. He was a Junior Research Fellow with the Department of Science and Technology and the Science and Engineering Research Board (DST-SERB), Government of India, New Delhi, India. He was a Postdoctoral Research Fellow with the Research Center for Wind Energy Systems, Kunsan National University, Gunsan, South Korea, from May 2017 to October 2018. He is currently working as a Postdoctoral Research Fellow with the Department of Mathematical Sciences, Shibaura Institute of Technology, Saitama, Japan. He has authored and coauthored of more than 35 research articles in various SCI journals. His research interests include complex-valued NNs, complex dynamical networks, control theory, stability analysis, sampled-data control, multi-agent systems, T-S fuzzy theory, and cryptography. He serves as a reviewer for various SCI journals.

**SABARATHINAM SRINIVASAN** was born in 1987. He received the bachelor's and master's degrees from the Rajah Serfoji Government College, affiliated by Bharathidasan University, India, in 2007 and 2009, respectively, and the M.Phil. and Ph.D. degrees from the Centre for Nonlinear Dynamics, School of Physics, Bharathidasan University, Tiruchirappalli, India, in 2011 and 2016, respectively. He was a National Postdoctoral Fellow (Principal Investigator) with the Department of Physics and Astrophysics, University of Delhi, New Delhi, India, funded by the DST Science and Engineering Research Board, Government of India. He is currently working as a Postdoctoral Research Fellow with the Aragon Institute of Engineering Research, University of Zaragoza, Spain. His research interests include nonlinear dynamics, chaos, transient chaos, complex networks, chaos in MEMS resonator, hidden attractor, memristive systems, delay dynamical systems, fractional order system, and controlling multistability.

**GUISHENG ZHAI** (Senior Member, IEEE) received the B.S. degree from Fudan University, China, in 1988, and the M.E. and Ph.D. degrees in system science from Kobe University, Japan, in 1993 and 1996, respectively. After two years of industrial experience, he moved to Wakayama University, Japan, in 1998, and changed to Osaka Prefecture University, Japan, in 2004. He held a Visiting Professor positions with the University of Notre Dame, from August 2001 to July 2002, and from March 2016 to February 2017, with Purdue University. In April 2010, he joined as a Faculty Member with the Shibaura Institute of Technology, Japan, where he is currently a Full Professor of Mathematical Sciences. His research interests include large scale and decentralized control systems, robust control, switched systems and switching control, networked control and multi-agent systems, neural networks, and signal processing. He is a member of ISCIE, SICE, JSST, and JSME. He is on the Editorial Board of several academic journals, including *IET Control Theory and Applications*, *International Journal of Applied Mathematics and Computer Science*, *Journal of Control and Decision*, *Frontiers of Mechanical Engineering*, *Science Nature*, and *Data Analytics and Applied Mathematics*.

**QIANG YU** (Member, IEEE) was born in Handan, Hebei, China, in 1979. He received the B.S. degree in mathematics education from Shihezi University, China, in 2003, and the M.S. degree in applied mathematics and the Ph.D. degree in basic mathematics from Shaanxi Normal University, China, in 2009 and 2014, respectively. From 2009 to 2011, he was an Instructor with Hengshui University. In July 2014, he joined Shanxi Normal University, China, where he is currently an Associate Professor with the School of Mathematics and Computer Science. Since August 2019, he has been a Visiting Professor with the Shibaura Institute of Technology, Japan. His research interests include stability of switched systems, positive systems, robust control, and time-delay systems.